Direct measurement of surface-state conductance by microscopic four-point probe method

2002 J. Phys.: Condens. Matter 14 8379

(http://iopscience.iop.org/0953-8984/14/35/309)

INSTITUTE OF PHYSICS PUBLISHING JOURNAL OF PHYSICS: CONDENSED MATTER

J. Phys.: Condens. Matter **14** (2002) 8379–8392 PII: S0953-8984(02)35066-5

Direct measurement of surface-state conductance by microscopic four-point probe method

Shuji Hasegawa[1], Ichiro Shiraki[1], Takehiro Tanikawa[1], Christian L Petersen[2], Torben M Hansen[3], Peter Boggild[3] and Francois Grey[3]

[1] Department of Physics, University of Tokyo, 7-3-1 Hongo, Bunkyo-ku, Tokyo 113-0033, Japan
[2] Capres A/S, DTU Bldg 404 East, DK-2800, Lyngby, Denmark
[3] 3 Mikroelektronik Centret, Technical University of Denmark, Bldg 345 East, DK-2800, Lyngby, Denmark

Received 20 March 2002, in final form 10 June 2002
Published 22 August 2002
Online at stacks.iop.org/JPhysCM/14/8379

Abstract

For *in situ* measurements of local electrical conductivity of well defined crystal surfaces in ultrahigh vacuum, we have developed microscopic four-point probes with a probe spacing of several micrometres, installed in a scanning-electron-microscope/electron-diffraction chamber. The probe is precisely positioned on targeted areas of the sample surface by using piezoactuators. This apparatus enables conductivity measurement with extremely high surface sensitivity, resulting in direct access to surface-state conductivity of the surface superstructures, and clarifying the influence of atomic steps upon conductivity.

1. Introduction

The topmost layers of crystal surfaces are known to have characteristic electronic band structures that are sometimes quite different from in the inner bulk. While such *surface states* have been well studied so far by, e.g., photoemission spectroscopy and scanning tunnelling spectroscopy, the electrical conduction through them, *surface-state conductance*, is little studied because of its difficulty [1]. Due to the thinness of the surface atomic layers, the surface-state conductance is usually much lower than the conductance through the bulk crystal. Furthermore, surface defects such as steps and domain boundaries greatly perturb the electron conduction through surface states. These facts have prohibited the direct detection and quantitative measurement of the surface-state conductivity. Since, however, the surface-state conductance, electron conduction through only one or two atomic layers, is a key and essential issue in the study of electronic transport in nanometre-scale regions or objects, it has recently attracted much interest, and large amounts of effort are now being exerted to detect and measure it. Here we introduce a novel tool, *a micro-four-point probe*, and also demonstrate its effectiveness for such a purpose [2–4].

First, we briefly introduce the four-point probe method and electrical conduction near a semiconductor surface. As shown in figure 1(a), the outer pair of probes touches a sample

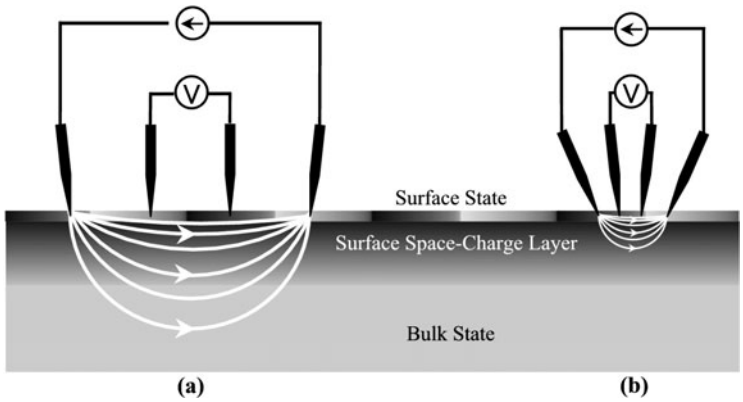

Figure 1. (a) Macro- and (b) micro-four-point probe method to measure electrical conductance. The distribution of current flowing through a semiconductor specimen is also schematically drawn.

surface and a voltage is applied between them, resulting in a current I flowing through the sample. The inner pair of probes picks up a voltage drop V along the surface due to the resistance of the sample. Thus one can obtain a four-probe resistance $R = V/I$ (strictly speaking, it is multiplied by a correction factor depending on the specimen shape and probe arrangement). Owing to this configuration, one can correctly measure the resistance of the sample without any influence of contact resistance at the probe contacts, irrespective of whether the probe contacts are ohmic or of Schottky type. This is because no current flows through the inner pair of contacts, so that no voltage drops at the probe contacts occur. This is a great advantage in the four-point probe method.

When the specimen is a semiconductor crystal, the measurement current will in principle flow through three channels in the sample [5]:

(1) *surface states* on the topmost atomic layers (when a well ordered surface structure is developed),
(2) bulk states in the *surface space-charge layer* beneath the surface (when the bulk bands bend under the surface, the carrier concentration can be different from in the inner bulk) and
(3) bulk states in the interior of crystal (which do not depend on the surface structures and states).

In general, the resistance measured by the four-point probe method contains the contributions from all of the three channels, and it is difficult to separate them. In the case of measurements in air the sample surface is usually dirty and does not have a well ordered surface structure, so the measured resistance is interpreted to be only the bulk value, but under special conditions where the bands bend sharply under the surface to produce a carrier accumulation layer, or in ultrahigh vacuum (UHV) where the sample crystal has a well defined surface superstructure to produce a conductive surface-state band, the contributions from the surface layers cannot be ignored. Even under such situations, however, the surface contributions have been considered to be very small, because, as shown in figure 1(a), the measurement current flows mainly through the underlying bulk in the case of *macroscopic* probe spacing.

Then, if one makes the probe spacing as small as the thickness of the space-charge layer or less, as shown in figure 1(b), the measurement current will mainly pass through only the surface region, which eliminates the bulk contribution from the resistance measurement. This

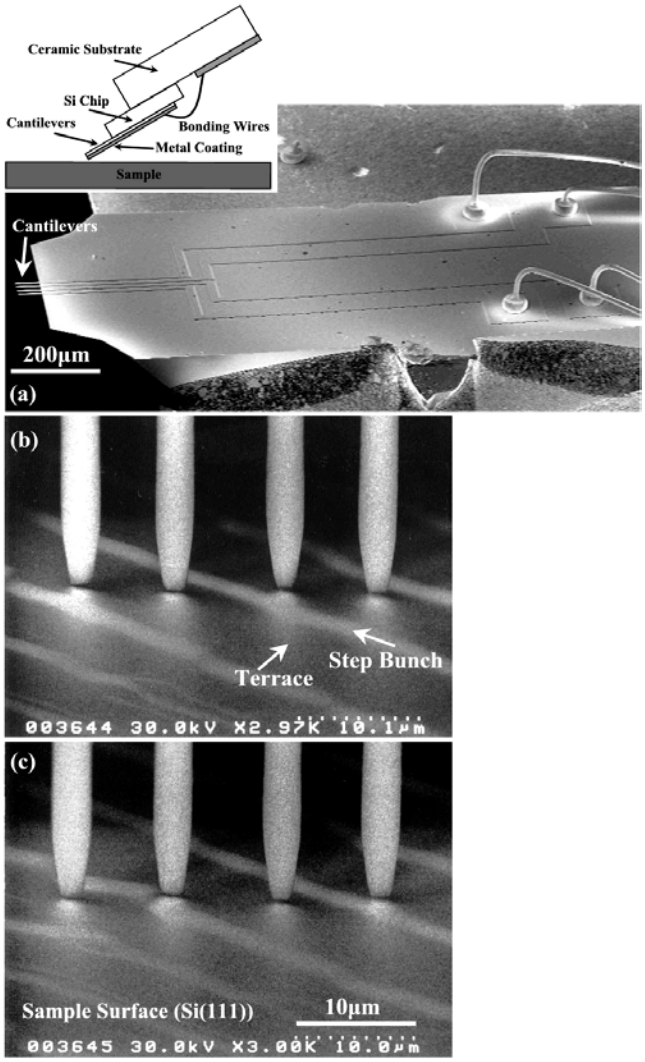

Figure 2. A micro-four-point probe. (a) SEM image of the chip. The inset shows a side view of the probe contacting a sample surface. (b), (c) Grazing-incidence SEM images of a micro-four-point probe (probe spacing being 8 μm), contacting a sample (Si(111)-7 $\times$ 7 clean surface) in UHV during measurement of conductance. The probe is shifted laterally from (b) to (c) by about 5 μm using piezoactuators for fine positioning.

microscopic four-point probe method thus has a higher surface sensitivity. This picture looks very naive, of course, because the real current distribution may be complicated due to a possible barrier between the surface state and bulk state and/or a possible pn junction between the surface space-charge layer and underlying bulk state, but the experimental results described below will qualitatively show the validity of this intuitive picture in figure 1.

Microscopic four-point probes have another advantage: they enable local measurements by selecting the area under concern with the aid of microscopes, so that the influence of observable defects can be avoided or intentionally included. Furthermore, by scanning the probes laterally on the sample surface, one can obtain a map of conductivity with a high spatial resolution [6].

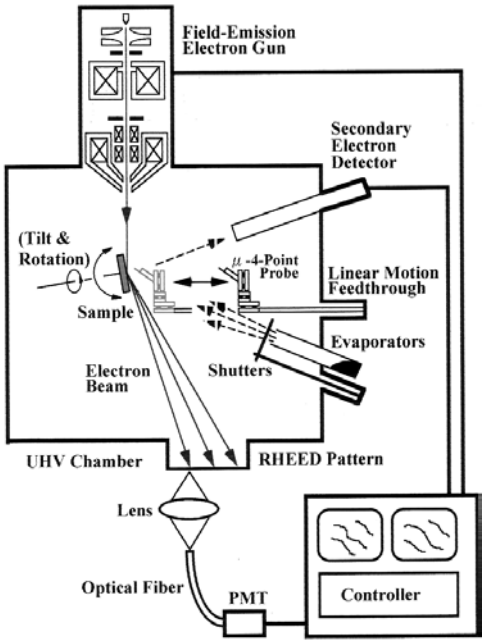

Figure 3. A schematic diagram of a UHV–SEM–RHEED system, combined with the micro-four-point probe system.

2. Experimental apparatus and method

Figure 2(a) shows a scanning electron micrograph (SEM) of a chip for the micro-four-point probe, which is produced by using silicon micro-fabrication technology in the Microelectronics Centre of Denmark Technical University [3]. The technique is similar to that for producing atomic force microscope cantilevers. The probes are now commercially available [7]. One can select a probe spacing ranging from 2 to 100 μm, while probes of several hundred nanometres spacing are under development. The substrate is an oxide-covered silicon crystal, on which a metal layer is deposited to make conducting paths. The metal layer covers the very end of four cantilevers so that they can make direct contact to the sample surface. The angle between the cantilever and sample surface is about 30°, as shown by the inset in figure 2(a), so that the cantilevers are bent to all contact to the sample easily even if the tips of the four cantilevers are not strictly aligned parallel to the sample surface.

This is installed in a UHV–SEM–RHEED (reflection-high-energy electron diffraction) chamber, as schematically shown in figure 3 [2]. Owing to a field-emission electron gun in the SEM column, this machine enables *in situ* characterization of the surface structures of sample by SEM, micro-beam-RHEED and scanning reflection electron microscopy (SREM) observations, as well as monitoring of the probe position. The sample surface can be cleaned by direct current heating, and materials can be *in situ* deposited from evaporators to prepare adsorbate-induced surface superstructures and epitaxial atomic layers on the specimen surface. Because of the glancing incidence of the electron beam, SEM images shown here are vertically shortened by a factor of about three compared with the horizontal direction in images.

The micro-four-point probe chip is moved away from the sample by using linear motion feedthrough during sample preparation. Then the chip is made to approach the sample with the coarse motion feedthrough, and final fine positioning is performed by three-axis piezoactuators

with a precision of about 10 nm to make contact to the targeted area on the sample under SEM observation.

Figures 2(b) and (c) are SEM images of a sample (Si(111)-7 × 7 clean surface) and the micro-four-point probe (8 μm spacing) contacting to the sample. The probe is shifted laterally by about 5 μm in figure 2(c) from the position in figure 2(b). In this way, the local conductance of the targeted areas can be measured by fine positioning of the probe with the aid of *in situ* SEM.

3. Surface sensitivity

We shall introduce some results for two typical surface structures on a Si(111) crystal. One is a Si(111)-7 × 7 clean surface, obtained by flash heating up to 1250 °C in UHV, and the other is a Si(111)-$\sqrt{3} \times \sqrt{3}$-Ag superstructure, obtained by depositing one atomic layer of Ag on the 7 × 7 surface kept at 450 °C. Their atomic arrangements and surface states are already well understood; the details are in, e.g., [1, 8]. The latter surface has a two-dimensional free-electron-like metallic surface-state band, while the former surface has a localized metallic surface state (dangling-bond state). These two surfaces thus provide comparative testing grounds for the surface conductance measurement.

Figures 4(a) and (b) show the results for the respective surfaces at room temperature (RT) in UHV obtained with a four-point probe of 8 μm spacing. The sample Si crystal was $3 \times 15 \times 0.4$ mm^3 in size, n-type, 10–100 Ω cm in bulk resistivity. The voltage drop measured by the inner pair of probes (in vertical axis) is linearly proportional to the current fed through the outer pair of probes (in horizontal axis). From the gradients of the curves, the differential resistance is obtained to be 120 ± 30 kΩ for the 7 × 7 surface and 400 ± 20 Ω for the $\sqrt{3} \times \sqrt{3}$-Ag surface. The error bars mean scattering depending on the measured areas on the respective surfaces.

Only one atomic layer of Ag deposited on a Si crystal 0.4 mm thick makes the electrical resistance decrease by more than two orders of magnitude! Many readers cannot believe this result at once, but we confirmed the reproducibility with several samples, and also confirmed that a micro-four-point probe of 20 μm spacing revealed similar results [3]. By comparing this result with the previous ones from macroscopic four-point probes of about 10 mm probe spacing in which the difference in resistance between the two surfaces was only around 10% [9], it is evident that the miniaturization of four-point probes makes the resistance measurements very sensitive to the surface structures. This is the expectation in figure 1. This result was further confirmed by the other type of four-point probe method, in which each of the four probes is independently driven to make the probe spacing change continuously from 1 mm to 1 μm [4, 10]. As the probe spacing is reduced, the difference in resistance between the two surfaces increases. The results with smaller probe spacing should be more intrinsic to the surface structures because of a more negligible contribution from the bulk region.

4. Surface-state conductance

The $\sqrt{3} \times \sqrt{3}$-Ag surface is thus shown to have a much lower resistance, or much higher surface conductance, than the 7 × 7 surface. Then, is this due to the surface-space charge layer or surface states? To answer this question, we shall first estimate the conductance through the space-charge layers under the respective surfaces. Since the Fermi-level position in the bulk is known from the impurity doping level (or the bulk resistivity), we have only to know the Fermi-level position at the surface (E_{Fs}). Then we can calculate the band bending beneath the surface and the resulting carrier concentration there, to obtain the conductance through

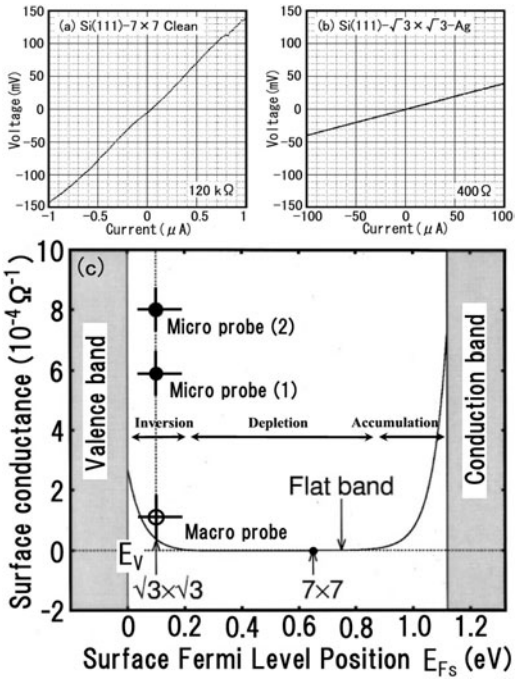

Figure 4. I–V curves measured at RT with the micro-four-point probe of 8 μm probe-spacing for (a) Si(111)-7 × 7 clean and (b) Si(111)-$\sqrt{3} \times \sqrt{3}$-Ag surfaces, respectively. By fitting the curve by a straight line, the differential resistance is obtained from its gradient. (c) The curve shows conductance through the surface space-charge layer, calculated as a function of the surface Fermi level position (E_{Fs}). The calculation is performed only for E_{Fs} within the bandgap. The conductance on the vertical axis is shown with respect to that under the flat-band condition. To compare this calculated conductance with the experimental data, first one has to know the E_{Fs} position of each surface, which has fortunately already been measured by photoemission spectroscopy. The E_{Fs}s for the 7 × 7 and $\sqrt{3} \times \sqrt{3}$-Ag surfaces are 0.63 eV and 0.1–0.2 eV above the bulk valence-band maximum E_V, respectively [12–14]. Since the calculated conductance is not an absolute value, but just a change from that under the flat-band condition, we cannot make a straightforward comparison between the calculated curve and the experimental data. Therefore, next we have to assume that the measured conductance of the 7 × 7 clean surface is the space-charge-layer conductance only; no surface-state conductance contributes. Then the data point of the 7 × 7 surface is right on the calculated curve at $E_{Fs} = 0.63$ eV from E_V. Since, then, we can obtain the difference in conductance between the 7 × 7 and $\sqrt{3} \times \sqrt{3}$-Ag from the measured conductance of the two surfaces, we can plot the conductance difference at the E_{Fs} position of the $\sqrt{3} \times \sqrt{3}$-Ag surface, which is indicated by black circles. The point indicated by 'Micro probe (1)' is a datum from (a) and (b), which was obtained with an 8 μm spacing probe on a Si(111) surface with a regular-step structure. Another data point indicated by 'Micro probe (2)' is the result obtained with 20 μm probe spacing on a terrace of an almost step-free region of a step-bunched surface (see the next section for the details) [3]. Both of the data points significantly deviate upwards from the calculated curve. Therefore, the high conductance of the $\sqrt{3} \times \sqrt{3}$-Ag surface is not explained only by the space-charge-layer conductance; rather, the surface-state conductance dominantly governs the measured value. If the assumption mentioned above about the conductance of the 7 × 7 surface is not true, that is, if the surface-state conductance greatly contributes to the measured conductance for the 7 × 7 surface, its data point should be located above the calculated curve. Then the data points for the $\sqrt{3} \times \sqrt{3}$-Ag surface also deviate further upwards above the calculated curve. This means again that the contribution from the surface-state conductance is larger. Therefore, the above assumption does not affect the conclusion of the surface-state conductance of the $\sqrt{3} \times \sqrt{3}$-Ag surface; rather, it makes an underestimation for the surface-state conductance. Though there are reports that the surface-state conductance of the 7 × 7 surface is 10^{-6}–10^{-8} Ω^{-1} [19, 20], the conductance is lower than that of the $\sqrt{3} \times \sqrt{3}$-Ag surface by two to four orders of magnitude, which is negligibly low. In any case, the conclusion about the $\sqrt{3} \times \sqrt{3}$-Ag surface is not affected by whether the surface-state conductance of the 7 × 7 surface contributes.

the surface space-charge layer [11]. The curve in figure 4(c) shows the space-charge-layer conductance calculated as a function of E_{Fs} for our sample crystal. The conductance on the vertical axis is shown with respect to that under flat-band conditions (where E_{Fs} coincides with E_F in the bulk). When E_{Fs} is located around the middle of the bulk bandgap, the surface space-charge layer is a depletion layer where the conductance is low. When E_{Fs} is near the bulk conduction-band minimum (valence-band maximum E_V), the layer is an electron (hole) accumulation layer where the conductance is increased due to the excess carriers in the layer. Fortunately, E_{Fs} positions at the 7×7 and $\sqrt{3} \times \sqrt{3}$-Ag surfaces are already known from photoemission spectroscopy measurements [12–14] to be 0.63 eV and 0.1–0.2 eV above E_V, respectively. These do not depend on the bulk doping level due to the Fermi-level pinning by metallic surface states. From figure 4(c), then, one can estimate the conductance through the surface space-charge layer below the respective surfaces. Since the 7×7 surface is located in the depletion region and the $\sqrt{3} \times \sqrt{3}$-Ag is in a weak hole-accumulation region, the latter surface should have a higher conductance than the former one. To compare this calculation result with the experimental data, the measured conductance for the respective surfaces is plotted in figure 4(c); a black dot (indicated by 'Micro probe (1)') shows the conductance of the $\sqrt{3} \times \sqrt{3}$-Ag surface with respect to that of the 7×7 surface, obtained from the data in figures 4(a) and (b). The data for the 7×7 surface are on the calculated curve: the details of data processing are described in the caption of figure 4. The data point for the $\sqrt{3} \times \sqrt{3}$-Ag surface is located significantly above the calculated curve, meaning that the measured high conductance of this surface cannot be explained only by the surface-space-charge-layer conductance; rather, the surface-state conductance contributes dominantly to the measured conductance.

The surface-state conductance of this surface has already been detected with the macroscopic four-point probe method by observing a conductance increase due to carrier doping into the surface-state band [15], but the micro-four-point probe method described above has made it possible just by comparing the conductance values between the two surfaces, due to its high sensitivity in measurements of the surface-state electrical conduction [3]. In spite of continuous efforts to detect the surface-state conductance since the 1970s, unambiguous experimental detections have been lacking for a long time [5]. Therefore, the results described above are of significant importance in surface physics, which opens a new opportunity to study the transport properties of surface electronic states.

For comparison, a result from a micro-four-point probe for a step-bunched Si(111)-$\sqrt{3} \times \sqrt{3}$-Ag surface is shown as another black dot (indicated by 'Micro probe (2)') in figure 4(c). This data point was obtained on a wide terrace under the condition that carrier scattering at surface atomic steps is minimal [3]. This data point also significantly deviates well above the calculated curve.

For further comparison, a data point obtained by a macro-four-point probe (probe spacing being about 10 mm) is plotted as an open circle in figure 4(c) [9]. Since this point is located close to the calculated curve, we could not say within the experimental errors that the data point deviates significantly from the calculated curve. Therefore, we could not conclude the contribution of the surface-state conductance just by comparing the measured conductance between the 7×7 and $\sqrt{3} \times \sqrt{3}$-Ag surfaces in the case of the macro-four-point probe method [9]. This is because the macro-probe method does not enable precise measurements of surface-state conductance because of inadequate surface sensitivity.

However, one may think that this reasoning is not convincing enough. Since, according to figure 4(c), the $\sqrt{3} \times \sqrt{3}$-Ag surface has an extremely high surface-state conductance compared with the conductance through the surface space-charge layer, one may claim that the surface-state conductance should be detected even by the macroscopic four-point probe method in spite of its low surface sensitivity, and its measured value should be the same as those obtained by the

micro-four-point probe method once the contribution from the bulk conductance is subtracted. Why does the measured surface conductance depend on the probe spacing?

According to Ohm's law in classical electromagnetism, when the resistance of an infinite two-dimensional sheet is measured by a linear four-point probe of probe spacing d, the measured resistance R is written as

$$R = (\ln 2/2\pi)R_S \tag{1}$$

where R_S is the sheet resistance. This means that the measured resistance should be constant, independent of the probe spacing d. This is because the carrier scattering centres are distributed densely; in other words, the spacing among the scattering centres is much smaller than the probe spacing, so R_S should be regarded as constant irrespective of the size of the measured area or probe spacing d. This evidently contradicts the data points in figure 4(c). Even if the average step–step separation is the same, the influence of step on resistance may depend on the degree of wandering of steps in macroscopic measurements; imagine that meandering steps may scatter the carriers more frequently than arrays of straight steps. However, when the conductance is measured in microscopic regions where the probe spacing is comparable to the distance between adjacent steps (i.e. terrace width), the steps should be regarded as straight in the measured area even if the steps are winding in a macroscopic scale. Therefore, the effective carrier scattering may be reduced. Thus the resulting sheet resistance R_S can be different depending on the scale of the measured areas. The conductance measured in microscopic regions should be an intrinsic value, due to reduction of the influence of atomic steps and other surface defects.

Next, let us estimate the mean free path L of the surface-state carriers. Since, as mentioned in section 3, the surface state of the $\sqrt{3} \times \sqrt{3}$-Ag has a nearly free-electron-like band in two dimensions, the sheet conductance $\sigma_{SS}(=1/R_S)$ is written in the Boltzmann picture as

$$\sigma_{SS} = S_F e^2 L/2\pi h \tag{2}$$

where S_F is the circumference of the Fermi disc ($S_F = 2\pi k_F$, k_F is the Fermi wavenumber), h is Planck's constant and e the elementary charge. Since k_F has already been measured by angle-resolved photoemission spectroscopy [15, 16], $k_F = 0.15 \pm 0.02$ Å^{-1}, S_F can be calculated. On one hand, we know $\sigma_{SS} = 8 \times 10^{-4}$ $\Omega^{-1}/\square$ from figure 4(c). Then, by substituting these values into equation (2), we obtain $L = 14 \pm 2$ nm for our sample at RT. This value is smaller than the typical step–step interval and domain size ($\sim$100 nm) by an order of magnitude, meaning that the surface-state carriers are scattered dominantly by phonons and surface defects other than atomic steps and domain boundaries. This means a diffusive conduction within single domains and terraces at RT. However, for the details of the carrier scattering mechanism, we have to measure the temperature dependence of conductance in a wide temperature range, for which we are now under preparation.

Next, let us estimate the mobility μ of surface-state carriers. The mean free path L can be written as $L = \tau V_F$, where τ is the relaxation time and V_F is the Fermi velocity. Since $V_F = \hbar k_F/m^*$, where m^* is the effective mass of surface-state carriers, V_F can be calculated, because we know m^* and k_F from the band dispersion measured by angle-resolved photoemission spectroscopy [15, 16], $m^* = (0.29 \pm 0.05)m_e$, where m_e is the free-electron mass. Then, we can estimate the relaxation time τ. Since the mobility μ is

$$\mu = e\tau/m^* \tag{3}$$

we can calculate $\mu = 140 \pm 40$ cm^2 V^{-1} s^{-1}. This value is lower than that of conduction electrons in three-dimensional bands of the Si bulk crystal, 1500 cm^2 V^{-1} s^{-1}, by an order of magnitude, meaning that the surface-state carriers are scattered by phonons and defects more seriously than the carriers in the bulk. It should be also noted that the mobility obtained here is higher than that obtained by the macro-four-point probe method by an order of magnitude [9].

This means, as mentioned above, that the influence of surface defects on carrier scattering is effectively reduced in microscopic measurements compared with macroscopic measurements. If one can measure the conductivity of almost defect-free regions with even smaller probes, the measured mobility will be further apparently increased.

Then, in the next section, we shall introduce the experimental results that directly show the influence of atomic steps upon the conductance.

5. Influence of atomic steps

On an usual nominally flat (111) surface of a Si crystal, atomic steps distribute regularly with a step–step distance of around 0.1–1 μm (regular-step surfaces). Therefore, to measure the step influence with micro-four-point probes of several μm probe spacing, step-free regions (terraces) should be made wider than the probe spacing by using a phenomenon of step bunching. Then the probes enable conductance measurements at terrace areas of almost step-free conditions or step-bunch areas with hundreds of steps accumulated, so that the influence of atomic steps upon conductance can be extracted by comparing the data for such regions.

Fortunately, a method for controlling the step configuration to obtain wide terraces has already been designed [17]. As shown in figure 5(a), arrays of small holes are made on a nominally flat (but actually slightly vicinal) Si crystal surface using suitable etching techniques before inserting the sample into UHV. The diameter and depth of the holes are around 1 μm, and their separation is around 20 μm in this case. When one repeats flash heating of the Si crystal up to 1250 °C in UHV by direct current flowing through the crystal in a direction perpendicular to the off angle direction, the sample surface is cleaned, and simultaneously the atomic steps move and the holes disappear as shown in figures 5(b) and (c). This is due to sublimation of Si atoms from the surface, resulting in moving back of atomic steps. With enough cycles of flash heating, finally, as shown in figure 5(d), atomic steps are accumulated at the positions of initial hole arrays, i.e. step bunches, between which wide and flat terraces of almost step-free conditions are created. The width of the terraces can be controlled by the initial hole-array separation; in figure 5, it is 20 μm, which is wider than the probe spacing. A step-bunch region contains around 300 monatomic steps separated by very narrow terraces, much like terraced fields on a mountain slope.

The sample surface in figures 2(b) and (c) was prepared with this method; brighter bands of about 2 μm wide running parallel to each other on the sample surface are step bunches, while darker areas of about 10 μm wide are flat terraces. In figure 2(b) a step bunch runs between the inner pair of probes, so that a voltage drop is measured across the step bunch, while in figure 2(c) the probes were shifted laterally to put the inner pair of probes on a single terraces with no step-bunch crossing. By comparing the measured resistances at these two positions, the result should contain more influence of steps under the former situation. In this way, the micro-four-point probe enables the conductance measurements of selected microscopic areas by precise positioning.

Figure 6 shows *in situ* SEM observation during Ag deposition on such a step-bunched Si(111)-7 $\times$ 7 clean surface (figure 6(a)) at 450 °C [8]. Bright thin lines begin to appear at the initial stage of deposition as shown in figure 6(b). The deposited Ag atoms migrate on the surface at 450 °C, and then are captured by atomic steps, where the 7 $\times$ 7 structure converts into the $\sqrt{3} \times \sqrt{3}$-Ag structure. The bright thin areas are the domains of the $\sqrt{3} \times \sqrt{3}$-Ag structure thus formed along steps, while darker areas are domains of the clean 7 $\times$ 7 structure. This image shows that the wide terrace areas of about 10 μm wide are not strictly step-free, rather several steps run across the wide terraces. However, this is a much lower step density compared with that at the step bunch areas, where more than 100 steps are accumulated.

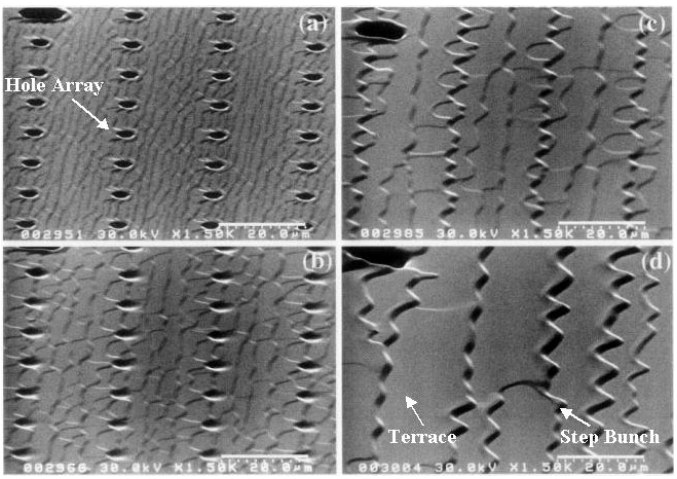

Figure 5. A series of *in situ* glancing-incidence UHV–SEM images, showing a process of step bunching on a Si(111) surface with small-hole array patterning. Repeating flash heating up to 1250 °C, the surface clearly becomes the 7 × 7 structure, and simultaneously atomic steps move back and are pinned at positions of the initial hole arrays.

With increase of Ag coverage, the brighter areas spread as seen in figures 6(c) and (c′), and simultaneously the $\sqrt{3} \times \sqrt{3}$-Ag domains appear on terraces as well as near step edges, as in figures 6(d) and (d′). Finally, with deposition of 1 ML of Ag, the terraces and step bunches are wholly covered by the brighter domains as shown in figure 6(e). By comparing with figure 6(a), the surface morphology of the terrace–step-bunch structure is not changed by the structure conversion from the 7 × 7 to $\sqrt{3} \times \sqrt{3}$-Ag. The narrow terraces in the step-bunch areas have the 7 × 7 and $\sqrt{3} \times \sqrt{3}$-Ag structures in (a) and (e), respectively, which are the same as the wide terrace areas.

Figures 7(a) and (b) show 'line profiles' of resistance measured with the micro-four-point probe (probe spacing = 8 μm) by shifting along a line across step bunches on such step-bunched Si(111)-7 × 7 clean and $\sqrt{3} \times \sqrt{3}$-Ag surfaces at RT, respectively. The horizontal axis shows the position of the probe on the line; the data points of measured resistance are plotted at the position of the centre of the micro-four-point probe. The error bars mean data scattering among several measurements on the same surfaces by repeating the retract and contact of the probe at each position. The surface morphology observed by SEM is schematically shown at the bottom of each graph (its vertical scale is exaggerated). These results show that the resistance changes drastically from place to place. As expected, when the inner pair of probes crosses over a step bunch as shown in figure 2(b) (such a situation occurs at dark shadow areas in figure 7), the measured resistance is higher. When the inner pair of probes contacts on the same terrace as shown in figure 2(c) without crossing a step bunch (such a situation occurs at bright shadow areas in figure 7), lower resistance values are obtained. The 7 × 7 and $\sqrt{3} \times \sqrt{3}$-Ag surfaces show qualitatively the same results, but they are quite different in the magnitude of change.

Since for the $\sqrt{3} \times \sqrt{3}$-Ag surface, as described in the previous section, the conductance is dominated by the surface state, the result in figure 7(b) means that the surface-state conduction is actually interrupted at step edges. This is very reasonable when one recalls STM pictures of so-called electron standing waves near step edges on this surface directly observed by low-temperature scanning tunnelling microscopy [18], which is nothing but the direct view of

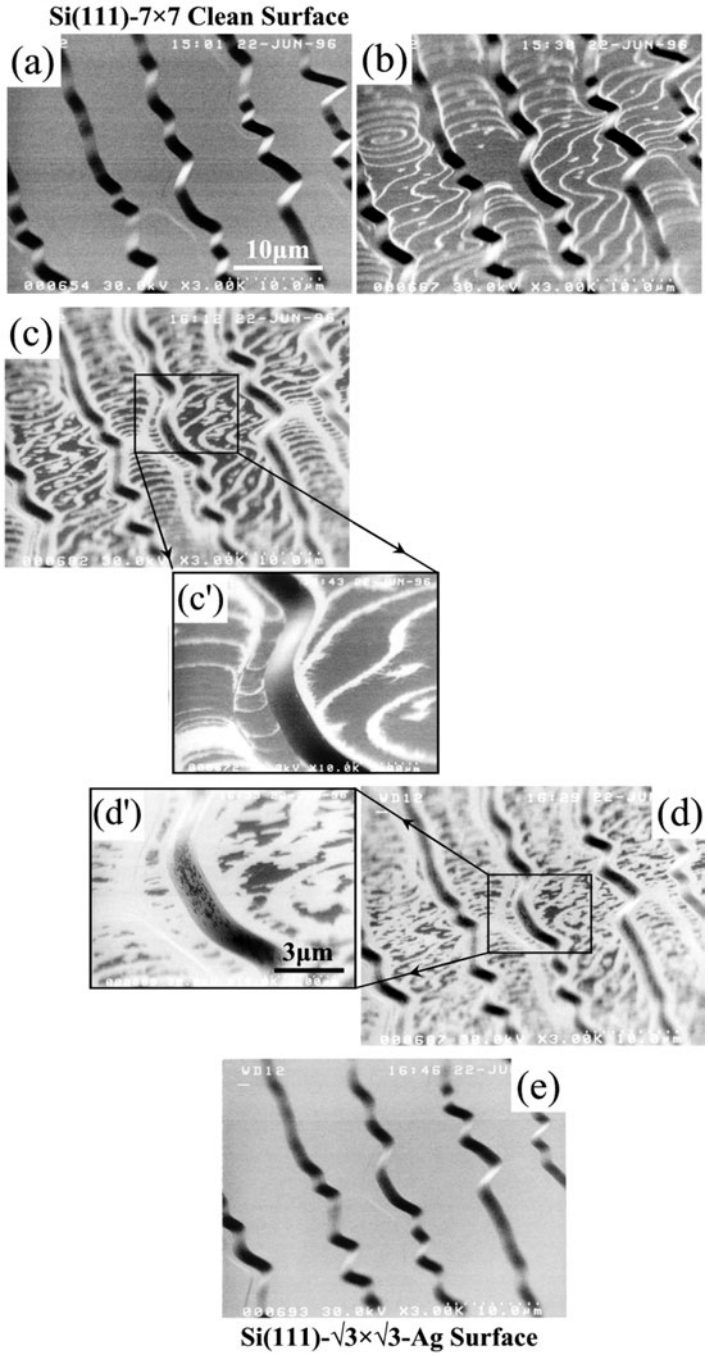

Figure 6. A series of *in situ* glancing-incidence UHV–SEM images during Ag deposition on a step-bunched Si(111)-7 × 7 clean surface kept at 450 °C. As Ag coverage increases, brighter thin domains ($\sqrt{3} \times \sqrt{3}$-Ag structure) appear at monatomic step edges and expand, while the darker domains (7 × 7 clean structure) shrink ((b)–(d)). Finally, the surface is wholly covered by the brighter domains homogeneously in (e). (c′) and (d′) are magnified images, showing that narrow terraces within step-bunch regions also change the structure. By comparing (a) with (e), it is noticed that the whole morphology of the surface does not change during this structure conversion.

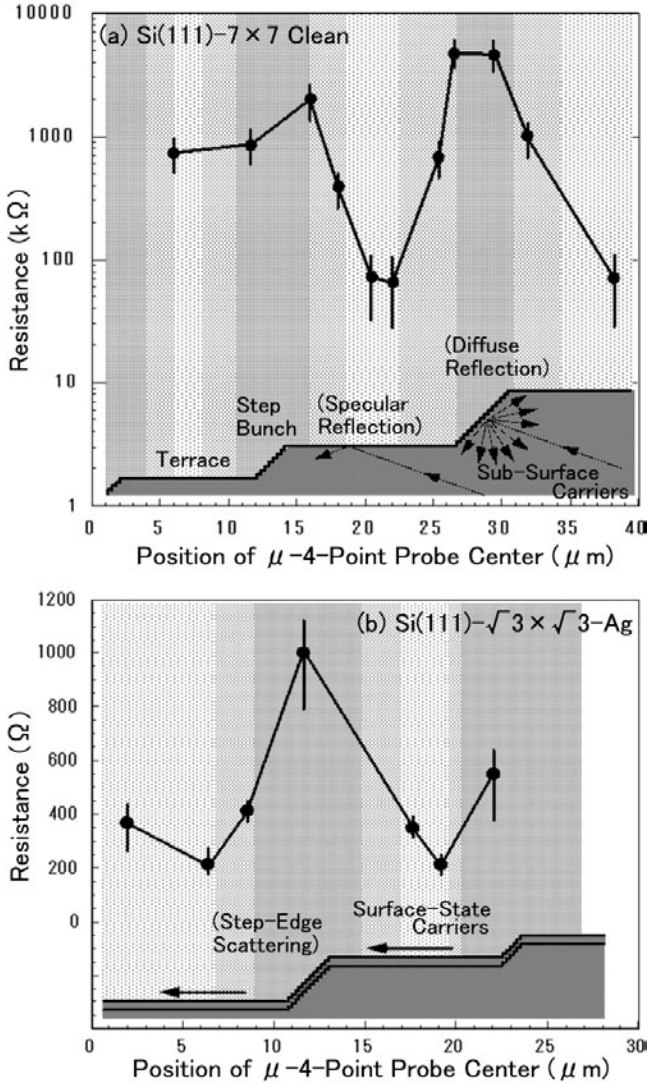

Figure 7. 'Line profile' of resistance of (a) Si(111)-7 × 7 clean and (b) Si(111)-$\sqrt{3} \times \sqrt{3}$-Ag surfaces, obtained by shifting the micro-four-point probes (8 μm probe spacing) along a line across step bunches on the surfaces. The surface morphology of sample surface, which is determined by SEM, is schematically drawn at the bottom of each graph. Areas of dark shadow show a situation where the voltage drop is measured by the inner pair of probes across a step bunch (as in figure 2(b)). Areas of light shadow show a situation where both of the inner probes contact on a single terrace (as in figure 2(c)); no step bunch runs between the inner probes. Areas of intermediate shadow show a situation where one of the inner probes is on a terrace and the other probe is on a step-bunch region.

carrier scattering at steps. Figure 7 is the first direct measurement of resistance caused by such step-edge scattering, from which we can deduce the resistance due to a single monatomic step and the transmission (and reflection) coefficient of the electron wavefunction of electrons there.

As shown in figure 4, the conductance of the 7 × 7 surface is lower than that of the $\sqrt{3} \times \sqrt{3}$-Ag surface by more than two orders of magnitude, which is reasonable when one recalls the reports about the surface-state conductance of the 7 × 7 surface [19, 20], giving it as 10^{-6}–10^{-8} Ω^{-1}. The surface-state electrical conduction is interrupted by steps in a similar

way as on the $\sqrt{3} \times \sqrt{3}$-Ag surface. The surface-space-charge-layer conductance is also low because of the depletion condition beneath the 7×7 reconstructed layer. The carriers flowing through the surface space-charge layer are also expected to be perturbed by the step bunches on the surface, because, according to the classical view of Fuchs and Sondheimer about carrier scattering at surfaces [21, 22], the carriers are scattered diffusively at the step-bunch areas because of the surface roughness as illustrated at the bottom of figure 7(a), while the carriers are reflected specularly at flat terraces. The diffusive scattering causes additional resistance, while the specular reflection does not. Alternatively, excess charges accumulated in electronic states characteristic to the step edges may locally disturb the band bending just below the step-bunch regions, resulting in carrier scattering in the surface space-charge layer. In this way, a higher resistance is most likely to be detected across the step bunches not only for the surface-state carriers, but also for the carriers flowing through the surface space-charge layer.

At this moment, we cannot detect the influence of a single atomic step upon the conductivity. It is still unclear whether the influence of a step bunch can be regarded as a simple multiple of the influence of a single atomic step. Strain fields are created near step bunches due to the narrow step–step distance in the step-bunch regions, which may cause additional influence on the conductivity.

Although the surface states are interrupted at step edges, the surface-state carriers can pass through the step edges with some probability, penetrating into the surface states on the adjacent terraces. The transmission probability at the step edges is less than 100%, but not zero. If the surface-state electrons have extended wavefunctions as for the $\sqrt{3} \times \sqrt{3}$-Ag structure, the transmission probability may be higher because of a larger overlap of wavefunctions with that on the neighbouring terraces. In contrast, the transmission probability may be lower for surface states having localized nature like that of the 7×7 surface, because of the negligible overlap of the wavefunction between the adjacent terraces, so the influence of steps upon the surface-state conductance may be more significant for the latter case. Actually, the resistance increases by two orders of magnitude at step-bunch regions for the 7×7 surface (figure 7(a)), while it increases by only a factor of four for the $\sqrt{3} \times \sqrt{3}$-Ag surface (figure 7(b)). Such an intuitive expectation should be confirmed by some theoretical estimation.

6. Concluding remarks

The micro-four-point probe described here is a quite unique and powerful tool for surface science, especially for study of surface transport, and is expected to be increasingly important because the electrical conduction through one or two atomic layers on surfaces may play essential roles in nanometre-scale science and technology. The reader can appreciate its usefulness from the preliminary results described here. Of course, the probe can be applied not only for study of surface transport, but also for transport properties of microscopic and nanometre-scale objects. The probe will be used under various conditions such as at low and high temperatures, under magnetic field and under light illumination. We have already constructed a system for the micro-four-point probe measurements at temperatures down to 10 K in UHV. The results will be reported elsewhere.

Acknowledgments

The present work was performed under a Grand-in-Aid from the Ministry of Education, Science, Culture and Sports of Japan, including the International Collaboration Program.

References

[1] For a review, see
Hasegawa S *et al* 1999 *Prog. Surf. Sci.* **60** 89
Hasegawa S *et al* 2000 *J. Phys.: Condens. Matter* **12** R463
[2] Shiraki I *et al* 2000 *Surf. Rev. Lett.* **7** 533
[3] Petersen C L *et al* 2000 *Appl. Phys. Lett.* **77** 3782
[4] For a review, see
Hasegawa S, Shiraki I, Tanabe F, Grey F and Oyo Buturi 2001 *Japan. Soc. Appl. Phys.* **70** 1165 (in Japanese)
[5] Henzler M 1975 *Surface Physics of Materials* vol 1, ed J M Blakely (New York: Academic) p 241
[6] Boggild P *et al* 2000 *Rev. Sci. Instrum.* **71** 2781
Boggild P *et al* 2000 *Adv. Mater.* **12** 947
[7] http://www.capres.com
[8] For a review, see
Hasegawa S *et al* 2000 *Japan. J. Appl. Phys.* **39** 3815
[9] Jiang C-S, Hasegawa S and Ino S 1996 *Phys. Rev.* B **54** 10 389
[10] Shiraki I *et al* 2001 *Surf. Sci.* **493** 643
[11] For fundamentals of semiconductor surfaces, e.g.
Moench W 1995 *Semiconductor Surfaces and Interfaces* (Berlin: Springer)
[12] Himpsel F J, Hollinger G and Pollak R A 1983 *Phys. Rev.* B **28** 7014
[13] Viernow J *et al* 1998 *Phys. Rev.* B **57** 2321
[14] Hasegawa S *et al* 1997 *Surf. Sci.* **386** 322
[15] Nakajima Y *et al* 1997 *Phys. Rev.* B **56** 6782
[16] Tong X *et al* 1998 *Phys. Rev.* B **57** 9015
[17] Ogino T 1997 *Surf. Sci.* **386** 137
[18] Sato N *et al* 1999 *Phys. Rev.* B **59** 2035
[19] Hasegawa Y *et al* 1996 *Surf. Sci.* **358** 32
[20] Heike S *et al* 1998 *Phys. Rev. Lett.* **81** 890
[21] Sondheimer E H 1952 *Adv. Phys.* **1** 1
[22] Fuchs K 1938 *Proc. Camb. Phil. Soc.* **34** 100